Paper ID APEN-MIT-2022_0623
Applied Energy Symposium: MIT A
+B July 5-8, 2022 • Cambridge, USA

Dynamic mode decomposition of impinging jet in a T-junction

Anqi Li
School of Energy and Power Engineering
Xi'an Jiaotong University
Xi'an, PR China
laq1147283222@163.com

Tong Li
School of Energy and Power Engineering
Xi'an Jiaotong University
Xi'an, PR China
tongli97@stu.xjtu.edu.cn

Mei Lin*
School of Energy and Power Engineering
Xi'an Jiaotong University
Xi'an, PR China
janeylinm@mail.xjtu.edu.cn

Qiuwang Wang
School of Energy and Power Engineering
Xi'an Jiaotong University
Xi'an, PR China
wangqw@mail.xjtu.edu.cn

Abstract—Thermal fatigue in a T-junction is of crucial importance issue for the coolant system of nuclear energy plants. The dynamic mode decomposition (DMD) is employed to analyze the snapshot data from simulation results with applying large eddy simulation (LES). The thermal mixing flow in a square T-junction is simulated at the impinging jet (M_R = 0.2). The temperature difference of hot and cold fluids is 15 K. The corresponding Reynolds number is about 20000. The results show that the frequency of the velocity modes is not equal to that of the temperature mode. The frequency of the temperature mode 1 is more than 40% higher than that of the velocity mode 1. The main spatial structures of the temperature field and the velocity field are alternately arranged along the trajectory of the branch fluid entering the main duct. The main coherent structure of the velocity field arrives at the bottom wall of x/D_m = 1, whereas for the temperature field, it basically appears in the region of x/D_m = 0.6 - 0.8. The negative structures of the velocity mode 1 induces the positive structures of the temperature mode 1. Also, the coherent structures of Modes 1 and 2 grow along the normal direction during downstream propagation.

Keywords—Dynamic mode decomposition, T-junction, Impinging jet, Frequency, Coherent Structure.

I. INTRODUCTION

Nuclear energy, as an important clean energy, has been attracted great attention for the scholars due to reducing carbon dioxide emission in the current era. Safety is a challenging issue for nuclear power plants. It is well known that T-junction is a common component of the coolant system used for the mixing of hot and cold fluids in nuclear power and process plants. Due to the large temperature difference between the two fluids, the thermal fluctuation of the T-junction is caused and transmitted to the pipe wall. If the wall is imposed by the thermal fluctuation for a long time, thermal fatigue failure of the wall is formed, which will further lead to pipeline cracks, causing safety incidents at the nuclear power plant [1]. Therefore, the thermal striping phenomena generated by thermal fluctuation needs to be fully understood, which is one of the most important issues concerned with the nuclear safety.

The thermal mixing mechanism in T-junctions has motivated researchers to conduct numerous experimental and numerical studies [2,3]. Hirota et al. [4] conducted an experiment to clarify turbulence mixing of two fluids with different temperature in a rectangular cross-flow type T-junction. The dominant structures of the velocity and concentration fields were extracted by proper orthogonal decomposition (POD). Su et al. [5,6] investigated turbulent thermal mixing flow in the T-junction under inflow pulsation by means of LES. Subsequently, some scholars have devoted to reduce the thermal fluctuation resulting from temperature difference to avoid the thermal fatigue formation of the pipeline [7].

Identification of coherent structures is of importance for understanding the dynamics feature of a fluid flow. Dynamic mode decomposition (DMD) is nowadays a powerful tool for the analysis of complex flows, which can reveal the spatial structures at a temporal spectral component [8].

It should be noted that the aforementioned literature on the T-junction did not study the turbulent coherent structures of the hot and cold fluids for understanding the phenomenology and dynamics of thermal mixing flow. In

this paper, the DMD method is used to identify the coherent structures in the T-junction at an impinging jet for in-depth recognizing the thermal striping mechanism. The momentum ratio is M_R = 0.2. The temperature difference of hot and cold fluids is 15 ℃. The instantaneous velocity and temperature fields are obtained by Large Eddy Simulation. Here, 1000 snapshots of velocity field and temperature field are used as the basic data of dynamic mode decomposition. The sampling start time is 25 s and the sampling frequency is 200 Hz, that is, the time interval of snapshots is 0.005 s. The velocity mode and temperature mode are analyzed from spatial scale and time scale.

II. DYNAMIC MODE DECOMPOSITION

Dynamic mode decomposition based on a data-driven algorithm reveals non-orthogonal spatial coherent structures (modes) with a single temporal spectral component, which was first proposed by Schmid [8]. More details on DMD can be found in [8], here, a brief introduction on the DMD is described as follows.

The flow field snapshots can be represented by a high dimensional matrix $\boldsymbol{X}$

$$\boldsymbol{X} = \{v_1, v_2, v_3, \dots v_n\} \tag{1}$$

where N is the number of sampling, v_i is the ith snapshot of flow field. The interval time between two adjacent snapshots is Δt.

The matrix X can be decomposed as $\boldsymbol{X_1}$ and its subsequent matrix $\boldsymbol{X_2}$ can be expressed as

$$\boldsymbol{X_1} = \{v_1, v_2, v_3, \dots v_{n-1}\} \tag{2}$$

$$\boldsymbol{X_2} = \{v_2, v_3, v_4 \dots v_n\} \tag{3}$$

Next, the flow field v_{i+1} at t_{i+1} can be connected by linearly operator $\boldsymbol{A}$ mapping from the flow field x_i at t_i, that is

$$v_{i+1} = \boldsymbol{A} v_i \tag{4}$$

Thus, two matrix $\boldsymbol{X_1}$ and $\boldsymbol{X_2}$ is also given by

$$\boldsymbol{A}\,\boldsymbol{X_1} = \boldsymbol{X_2} \tag{5}$$

A matrix $\boldsymbol{S}$ can be obtained by

$$S \equiv V^H \boldsymbol{A} V = V^H \boldsymbol{X_2} W \Sigma^{-1} \tag{6}$$

The matrix $\boldsymbol{S}$ is similar to $\boldsymbol{A}$ that is the approximation of $\boldsymbol{A}$ in the column space of $\boldsymbol{X}_1$. The modes obtained by dynamic mode decomposition are time orthometric, mode frequency and growth rate can be calculated by the eigenvalue of A, as

$$\omega_i = Im[lg\ \mu_i / \Delta t]$$

$$R = Re\left[\frac{lg\ \mu_i}{\Delta t}\right] \tag{7}$$

The original system can be represented by:

$$\begin{aligned} X_1 &= [v_1, v_2, v_3, \cdots, v_{N-1}] \\ &= \boldsymbol{\Phi D}_{\alpha} \boldsymbol{V}_{and} \\ &= [\boldsymbol{\Phi}_1, \boldsymbol{\Phi}_2, \boldsymbol{\Phi}_3, \cdots, \boldsymbol{\Phi}_r] \times \begin{bmatrix} \alpha_1 & & & \\ & \alpha_2 & & \\ & & \ddots & \\ & & & \alpha_r \end{bmatrix} \begin{bmatrix} 1 & \mu_1 & \dots & (\mu_1)^{N-2} \\ 1 & \mu_2 & \dots & (\mu_2)^{N-2} \\ \vdots & \vdots & \ddots & \vdots \\ 1 & \mu_r & \dots & (\mu_r)^{N-2} \end{bmatrix} \end{aligned} \tag{8}$$

where the Vandermonde matrix $\boldsymbol{V}_{and}$ composed of eigenvalues of $\boldsymbol{A}$ indicates the time evolution of the flow field. α_i represents the amplitude of the ith mode, which also represents the modal contribution on the initial snapshot.

III. NUMERICAL SIMULATION

A. Physical model

Fig. 1 depicts the physical model that is a square cross-section T-junction with the main duct of D_m = 100 mm and the branch duct of D_b =50 mm. The diameter ratio of both ducts is D_m/D_b = 2. In the Cartesian coordinate system, hot water of 48 ℃ and cold water of 30 ℃ flows along the main duct (x-axis) and the branch duct (negative z-axis), respectively. The origin of coordinates is set at the AD line of the bottom wall (Face ABCD) and the corresponding center face of the branch duct. The two inlets for the main duct and branch duct are set at 10 hydraulic diameters upstream of the T-junction to ensure the fully developed flow, respectively. The outlet of the main duct is at x = 20 D_m. Flow snapshots are collected at the dashed box from x = 0 to 3.5 D_m, shown in Fig. 1 (b).

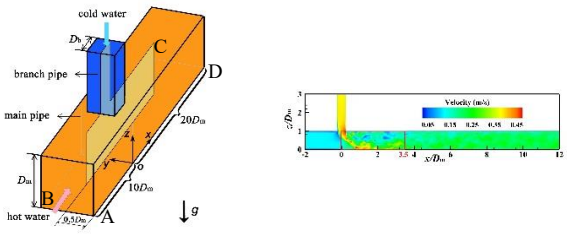

(a). Overall schematic (b). Snapshot area (y/D_m = 0.5)

Fig. 1. Physical model and snapshot area (not to scale)

B. *Numerical setup*

The large eddy simulation model is used to simulate the thermal mixing flow of hot and cold fluids in the T-junction at the impinging jet. Its basic principle is to separate the large-scale eddy and the small-scale eddy of the governing variable through filtering. The large-scale eddy is solved by the filtered Navier-Stokes equations directly. While the sub-grid scale model is conducted to deal with the small-scale eddy that is resolved by the wall-adapted local eddy-viscosity (WALE) sub-grid scale model. The governing equations based on continuity, momentum and energy conservation for incompressible unsteady flow are omitted here due to limited space. The details can be found in [12]. Also, the grid independence and model validation can be found in Ref. 12. The calculation boundary conditions of two inlets are list in TABLE I. The momentum ratio is $M_R = 0.2$, and the velocity of the main fluid is 0.11 m/s and that of the branch fluid is 0.35 m/s, the corresponding Reynolds numbers are 19077 and 22990, respectively. The temperature difference of two fluids is 15 K.

TABLE I. CALCULATION CONDITIONS FOR IMPINGING JET.

Inlet	Velocity (m/s)	Temperature (K)	*Re*	M_R
Main duct	0.11	321.15	19077	0.2
Branch duct	0.35	306.15	22990	0.2

IV. RESULTS AND DISCUSSION

1000 snapshots of the velocity field and the temperature field are extracted from the results of LES separately with a constant sampling frequency 200 Hz from 25.001 to 29.996 s.

A. *DMD mode of velocity field*

Fig. 2 plots the velocity field of the impinging jet in a T-junciton at the symmetrical plane *x-z* section, $y/D_m = 0.5$, including the time growth rate *R* of the 40-order modes sorted from small to large frequency, and the actual dimensionless physical frequency St. 429 or 215th-order modes are reserved by the optimal truncated singular value solution for calculation, and the frequency St ranges from about -9.89 to 9.89. The growth rate *R* is widely distributed between -611.27 and 0.28, and most of them are negative value, their absolute value is less than 0.8.

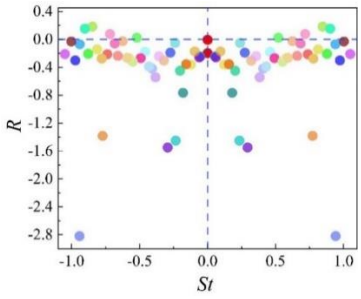

Fig. 2. Part of the dynamic modal spectrum of the velocity field

The growth rate filtering method (GRF) is used to sort the modes, and the maximum velocity difference is 0.57 in the velocity field at the inlet impinging jet, so the growth rate threshold Rth is about 0.11 under this condition. The more stable modes are screened according to the growth rate threshold Rth. Fig. 3 shows the energy values of all modes after screening, and they are sorted according to the energy values of each mode. The modes marked in color in the figure are the first 6 modes that contribute more to the system.

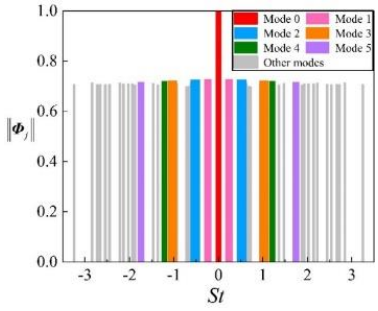

Fig. 3. Energy values of the modes of the velocity field

TABLE II lists the eigenfrequencies and growth rates corresponding to the first 6 modes. The energy value of mode 0 is 1, its frequency is zero, and the growth rate is approximately 0, which means that its structure hardly changes with time. The eigenfrequency of mode 1 with higher energy value can be considered as one of the main frequencies of the system, and its St value is about 0.23. At the same time, the eigenfrequencies of modes 2-4 are basically multiples of the frequencies of mode 1, and the multiple relationship will be reflected in the special spatial structure of the modes. From mode 0 to mode 5, the eigenfrequency value gradually increases, and the energy

value decreases slightly, which indicates that the structural energy has a decay process as the frequency increases.

Fig. 4 shows the spatial coherence structure of the first six dynamic modes of the velocity field at t = 26.05 s. Red represents positive values of $\boldsymbol{\Phi}_j$ energy and blue means negative values of $\boldsymbol{\Phi}_j$. Mode 0 is the dominant flow structure of the original flow field of the impinging jet at y/D_m = 0.5, named as the time-average velocity mode with the frequency of zero, shown in Fig. 4(a). The original velocity field can be regarded as the superposition of oscillation modes of different frequencies on Mode 0. The colour transition is uniform and smooth. The flow state of the branch jet rushing to the bottom wall of the main duct can basically be seen, and almost no small-scale structure can be observed in Mode 0 as expected. The other modes show more complex and small spatial structure features in the T-junction which are associated with different frequencies.

TABLE II. TIME INFORMATION OF VELOCITY FIELD

Mode	$\|\boldsymbol{\Phi}_j\|$	*St*	*R*
0	1	0	-5.8E-3
1	0.729	0.23	-0.05
2	0.726	0.52	0.02
3	0.722	1.03	-0.01
4	0.721	1.21	-0.01
5	0.716	1.75	0.01

Fig. 4(b-f) shows the spatial coherent structures of Modes 1-5 of the velocity field in the T-junction. It can be seen that the positive and negative structures are arranged along the impact angle of the branch jet, the dashed line is the propagation path line. In Modes 1 and 2, there are multiple concentric arcs composed of positive and negative coherent structures that spread in the whole section from the upper wall to the bottom wall. These coherent structures increase along the normal direction (z-axis). The negative structures of Mode 1 dominant the velocity fluctuation. When these structures propagate to the bottom wall of the main duct at the position of x/D_m = 1, they are tangent to the bottom wall and then develop counterclockwise to the positive direction of the z-axis, which can be considered that these coherent structures produce due to the cold fluid in the branch duct impinging the bottom wall of the main duct, whose modal energy before contacting the bottom wall is greater than that after contacting the bottom wall, reflecting the energy dissipation caused by the impinging jet.

The structures of Modes 3-5 are similar, they are also distributed along the jet impingement direction to x/D_m = 1, and then develop along the direction parallel to the wall. The maximum energy appears at the beginning of the branch fluid entering the main duct at z/D_m = 0.6 - 0.8 except of Mode 3, and at the position of x/D_m = 1 - 1.5 and z/D_m = 0.2 - 0.4 after contacting the bottom wall. As the mixing strength of different fluids in the x-axis direction decreases, the modal energy decreases and continues to be aligned parallel to the bottom wall. The three modes indicate that the modal energy decreases as the eigenfrequency increases.

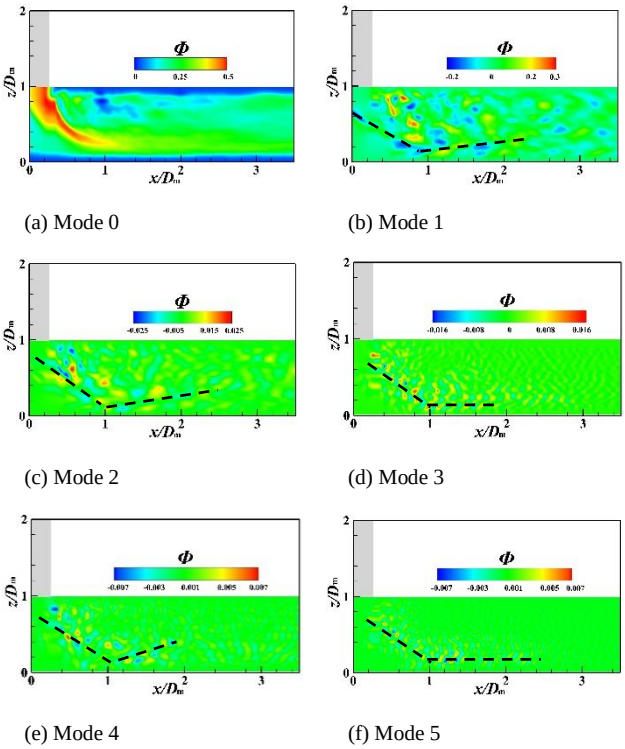

(a) Mode 0 (b) Mode 1

(c) Mode 2 (d) Mode 3

(e) Mode 4 (f) Mode 5

Fig. 4.Spatial modes of the velocity field at the impinging jet at t = 26.051 s

B. DMD mode of temperature field

The GRF modal sorting method is used to screen and sort the dynamic modes of the temperature field. Since the temperature of the hot and cold fluids remains unchanged in

this paper, the difference is always 15 K. Therefore, the growth rate threshold R_{th} is 3.

Fig. 5 lists the time growth rate R and the actual dimensionless physical frequency St of the 40th order modalities of the temperature field at y/D_m = 0.6 in the T-junciton at the impinging jet. The optimal truncated singular value solution is used to retain 458 or 229th-order modes for calculation. The range of frequency St is about -12.12 to 12.12, and the frequency distribution range is much larger than the temperature field of wall jet and deflected jet; the value of growth rate R is widely distributed between -322.13 and 0.47, most of the modal growth rates have small absolute values and are concentrated around R = 0.

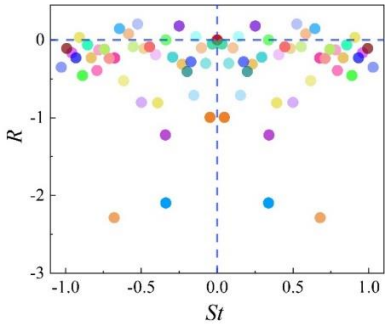

Fig. 5.Partial dynamic modal spectrum of temperature field

Fig. 6 shows the energy values of all modes after the temperature field at the impinging jet is screened, sorted according to the energy value of each mode. The modes marked in color in the figure are the first 6 modes that contribute more to the system. Table 3 lists the time information for the main modes of the temperature field. The modal eigenfrequencies of temperature field in the T-junction are approximately 0.33, 0.58, 0.85, 1.40, and 1.87, and slight higher than that of velocity field, respectively. Mode 0 is still the most stable mode with a growth rate R = -2.60E-5, which is the average mode of the temperature field. The energy of each mode decreases with increasing eigenfrequency. Due to the large threshold for the growth rate of the temperature field, the growth rates of the main modes in this group of data are all around 0.70, and they are all positive values. It can be considered that the spatial structure of Modes 1-5 is increasing with time. The main modal eigenfrequency is about a multiple of 0.33, and the modal eigenfrequency of the temperature field of the stable inlet impinging jet is 30% greater than the velocity field eigenfrequency.

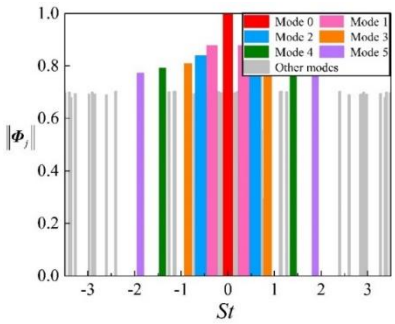

Fig. 6.Energy value of the modal of the temperature field at t = 26.051 s

TABLE III. TIME INFORMATION OF VELOCITY FIELD

Mode	$\|\Phi_j\|$	St	R
0	1	0	-2.60E-5
1	0.879	0.33	0.72
2	0.839	0.58	0.72
3	0.811	0.85	0.70
4	0.792	1.40	0.71
5	0.773	1.87	0.70

Fig.7 shows the spatial coherence structure of the first six modes of the temperature field at t = 26.051s. Red and blue repreaent the high temperature fluctuation and low tempearature fluctuation, respectively. Mode 0 is the time-average mode of temperature field at the impinging jet at y/D_m = 0.5, shown in Fig. 7(a). It can be seen that the hot and cold fluids start to mix from z/D_m = 0.8, x/D_m = 0, and the temperature field is basically uniform at x/D_m = 1; at the same time, it can also be observed that a thermal mixing structure of hot fluid appears near the upper wall when the branch jets enter the main duct. The coherent structures of Modes 1-5 are plotted in Fig. 7 (b-f), and similar to that of the velocity field, evolve along the cold fluid flow trajectory and disappear at x/D_m = 2. As obeserved carefully, in Fig. 7b, the coherent structure of Mode 1 mainly distribute the thermal mixing layer and the region of x/D_m = 2 from the upper wall to the bottom wall, indicating that the coherent structures diffuses in the normal direction (z-axis) as it propagates downstream in the T-junction. The positive structure dominants the

temperature fluctuation of a T-junction at the impinging jet. The energy values of the coherent strucutres gradually weaken along the positive direction of the *x*-axis. The coherent structure of Mode 2 is circular, shown in Fig. 6c, and moves along the upstream side as well as the non-obvious growth along the normal direction. Modes 3-5 basically flow along the tributary trajectory, and as the eigenfrequency increases, the structure from Mode 3 to 5 extends into a slender strip. In addition, the coherent strutures of Mode 5 with low energy value mainly propagate downstream along the backflow side, that is, a part of high energetic positive and negative structures is distributed in the region from $z/D_m \leq 0.4$ and $x/D_m = 0.4$ - 1.6. Compared with the velocity field, the main coherent structure of the temperature field change the direction of movement in the region of $x/D_m = 0.6$ - 0.8, this is because the thermal mixing starts at the moment when the cold fluid enters the main pipe, and the velocity mixing appears at the boundary of two fluids with different velocities, so the coherent structure of the velocity field appears at the boundary of the branch fluid.

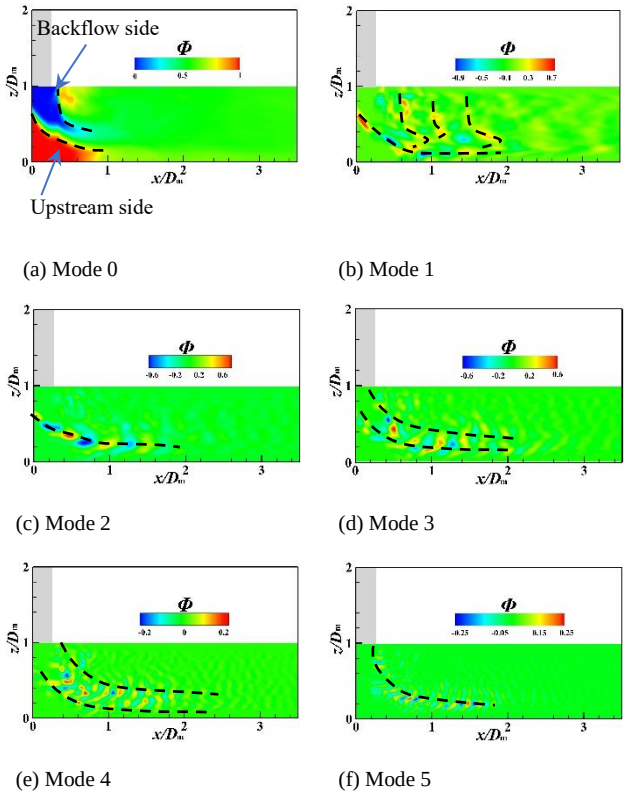

(a) Mode 0 (b) Mode 1

(c) Mode 2 (d) Mode 3

(e) Mode 4 (f) Mode 5

Fig. 7. Spatial modes of the temperature field at t = 26.051 s

V. CONCLUSIONS

In this paper, the dynamic mode decomposition (DMD) is employed to investigate the data resulting from the thermal mixing flow in a square T-junction at the impinging jet simulated by large eddy simulation (LES). The momentum ratio is 0.2. The main conclusions are drawn in the following:

The main spatial structures of the velocity field and the temperature field are mostly composed of positive and negative structures alternately arranged along the trajectory of the branch fluid entering the main duct; the main coherent structure of the velocity field arrives at the bottom wall of x/D_m = 1, whereas for the temperature field, it basically appears in the region of x/D_m = 0.6 - 0.8. For Mode1, the negative structures of the velocity field dominant the fluctuation, while the positive structures of the temperature field favors its degree of mixing between the hot and cold fluids. These coherent structures of Mode 1 and 2 spread in the whole T-junction,while for the rest modes, they are located at the bottom wall. Also, the frequency of the velocity Mode 1 is 30% smaller than that of the temperature Mode 1.

ACKNOWLEDGEMENT

This work was financially supported by the National Natural Science Foundation of China (Grant No. 51976159).

REFERENCES

[1] O. Gelineau, C. Escaravage, J.P. Simoneau, and C. Faidy, " High cycle thermal fatigue: experience and state of the art I French LMFRs," in Proceeding of 16th International Association for Structural Mechanics in Reactor Technology (SMIRT-16). Washington DC, United States, Aug. 12-17 2001.

[2] H. Kamide, M. Igarashi, S. Kawashima, N. Kimura, and K. Hayashi, " Study on mixing behavior in a tee piping and numerical analyses for evaluation of thermal striping," Nucl. Eng. Des. 239, pp.58-67, 2009.

[3] M. Georgiou, and M. V. Papalexandris, "Direct numerical simulation of turbulent heat transfer in a T-junction," J. Fluid Mech. 845, pp.581-614, 2018.

[4] M. Hirota, E. Mohri, H. Asano, and H. Goto, "Experimental study on turbulent mixing process in cross-flow type T-junction," Int. J. Heat Fluid Flow 31 (5), pp. 776-784, 2010.

[5] B. Su, Z.L. Zhu, H.B. Ke, Q.W. Wang, and M. Lin, "Large eddy simulation of flow and mixing characteristics in a T-junction under inflow pulsation," Appl. Therm. Eng. 181, 115924, 2020.

[6] B. Su, Z.L. Zhu, X.Y. Wang, H.B. Ke, M. Lin, and Q.W. Wang, "Effect of temperature difference on the thermal mixing phenomenon in a T-junction under inflow pulsation," Nucl. Eng. Des. 363, 110611, 2020.

[7] K. X. Huang, B. Su, T. Li, H. B. Ke, M. Lin, and Q. W. Wang, "Numerical simulation of the mixing behaviour of hot and cold fluids in the rectangular T-junction with/without an impeller," Appl. Therm. Eng. 204, 117942, 2022

[8] P. J. Schmid, L. Li, M.P. Juniper, and O. Pust, "Applications of the dynamic mode decomposition," Theor. Comp. Fluid Dyn. 25, pp.249-259, 2011.